Journal of Materials Chemistry B

Accepted Manuscript

ROYAL SOCIETY OF CHEMISTRY

www.rsc.org/materialsB

Journal of
Materials Chemistry B

ARTICLE

Smart pH-responsive and high doxorubicin loading nanodiamond for in vivo selective targeting, imaging, and enhancement of anticancer therapy

Lin Li,[a] Lu Tian,[b] Yongli Wang,[d,e] Wenjing Zhao,[b] Fangqin Cheng,[c] Yingqi Li*[a,b] and Binsheng Yang*[a]

Received 00th January 20xx,
Accepted 00th January 20xx

DOI: 10.1039/x0xx00000x

www.rsc.org/

Nanodiamond as a carrier for transporting chemotherapy drugs has emerged as a promising strategy for treating cancer. However, several factors limited its extensive applications in biology, such as low drug loading, easily cluster and a high drug loss under physiological environment. In this work, to ensure high drug capacity and low drug leakage in physiological conditions, and especially ensure to be delivered to tumor region, a smart pH-responsive drug delivery system was designed and prepared by DOX adsorbed onto PEGylated nanodiamond in sodium citrate medium (ND-PEG-DOX/Na_3Cit, NPDC). The system can significantly enhance cellular uptake to exert therapeutic effect in comparison to free drug. And more importantly, DOX was released in a sustained and pH-dependent manner and exhibits excellent stability under neutral conditions. In addition, NPDC could enter into cells via both clathrin and caveolae-mediated endocytosis pathway, and then dissociated DOX migrated into nucleus to block the growth of cancer cells. Furthermore, NPDC can significantly inhibit the cell migration and change the cell cycle. Excitingly, the NPDC system was very smart to enrich at the tumor site in vivo effectively and to enhance antitumor efficiency with low toxicity beyond conventional DOX treatment in cancer cells and nude mouse model. So this study introduces a simple and effective strategy to design a promising drug delivery platform for improving the biomedical applications of the smart nanodiamonds carriers.

Introduction

Widespread tobacco use and unhealthy lifestyles, contributed to cancer becoming a major problem in the world.[1,2] In order to overcome the hot potato and improve the quality of life of patients around the world, drug development for cancer treatment is urgent and important. As far, about eighty kinds of anti-cancer drugs were used in clinical treatment, such as methotrexate,[3] camptothecin,[4] doxorubicin hydrochloride.[5] Among them, doxorubicin (DOX), with the trade name Adriamycin, is one of the most commonly used chemotherapeutic drugs.[6]

Unfortunately, cumulative chronic toxicities, poor bioavailability, and emergence of drug resistance in patients limited the biological application of DOX.[7-9] In order to reduce these toxic and side effects, many researchers have employed some drug delivery systems to improve the utilization and overcome the drawbacks of DOX. For example, Vijayakameswara etal. synthesized the amphiphilic block copolymer (COPY-DOX), as an efficient drug delivery system to interact with living organisms.[10] Fan. etal. developed a new multifunctional anticancer prodrug system based on water-dispersible fullerene aggregates, which exhibited active targeting, pH-responsive chemotherapy, and photodynamic therapeutic (PDT) properties.[11] However, in their studies, the drug release in tumor microenvironment was not satisfied with our expectation and the antitumor activity of the complexes was no match for the free DOX.

Nanodiamond (ND) has recently attracted significant attention in biological application,[12-20] owing to its better biocompatibility, optical properties, chemical stability and surface easily modified.[21-31] However, ND has a serious trend to aggregate to influence its application.[32] In order to overcome this defect, some proteins and polymers were introduced onto ND to improving dispersibility.[33-35] Among the polymers, especially poly (ethylene glycol) (PEG) is widely used due to excellent water-solubility and biocompatibility.[36-39] Therefore, PEG has been introduced to the ND, which can not only improve the dispersion, but also reduce the interaction with cells to reducing non-specific effects, and prolong the blood circulation time.[40-41] We have prepared ND-PEG via an ester band and found that PEGylated ND showed enhanced dispersity and stability in vitro under the physiological environment or in cell culture medium in our previous study.[42] Unfortunately, the amount of loaded DOX is relative poor and the drug dissociation in physiological environment is slightly high.

[a]Key Laboratory of Chemical Biology and Molecular Engineering of Ministry of Education, Institute of Molecular Science, Shanxi University, Taiyuan 030006, PR China. *E-mail: wkyqli@sxu.edu.cn, yangbs@sxu.edu.cn
[b]Department of Chemistry, College of Chemistry and Chemical Engineering, Shanxi University, Taiyuan 030006, PR China.
[c]Institute of Environmental Science, Shanxi University, Taiyuan 030006, PR China.
[d]Drug Safety Evaluation Center, China Institute for Radiation Protection, Taiyuan 030006, PR China.
[e]Shanxi Key Laboratory of Drug Toxicology and Drug for Radiation Injury, Taiyuan 030006, PR China.

Electronic Supplementary Information (ESI) available: [Stability, TEM, cell viability with time, cell morphology and cellular uptake kinetics]. See DOI: 10.1039/x0xx00000x

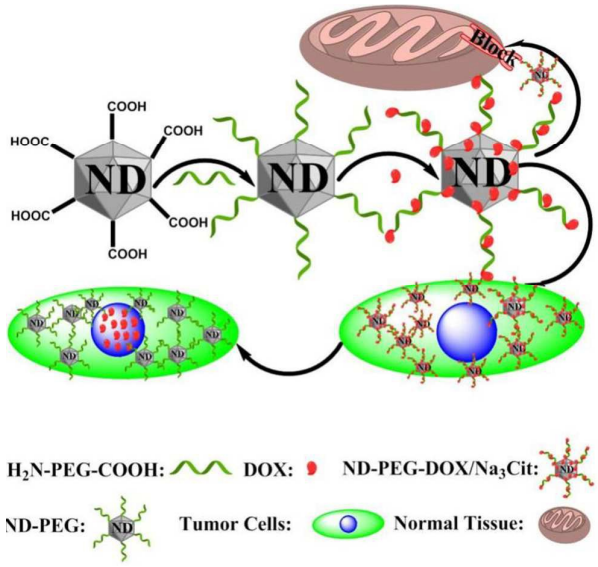

Scheme 1 Schematic illustration of the fabrication of an intracellular pH-responsive NPDC delivery system for cancer therapy.

Taking into account the necessity of high drug loading, augmented treatment efficiency and targeting ability for tumor, a novel nanodrug based on free DOX physical adsorption onto PEGylated ND in sodium citrate medium was designed (Scheme 1). Specifically, carboxylated ND was conjugated by polyethylene glycol amine carboxyl (H_2N-PEG-COOH) to obtain the ND-PEG-COOH nanocarrier. In the following step, DOX was successfully coated onto the ND-PEG-COOH in the sodium citrate medium via hydrogen bonds and van der Waals´ forces, to obtain ND-PEG-DOX/Na_3Cit (NPDC) nanoparticles. We found that the addition of Na_3Cit is an essential component of the loading process and the salt was shown to be able to promote the adsorption of DOX onto the PEGylated NDs, where about 85wt % adsorption of DOX added on the ND-PEG-COOH was achieved in the sodium citrate medium (Na_3Cit, 1.0 M). The NPDC was found to move inside the cells quickly and was capable of delivering the drug inside living cells efficiently. In addition, NPDC showed a higher cytotoxicity with time increased than that of the free DOX. Excitingly, the smart NPDC system was very effective in enrichment at the tumor site by both in vivo and ex vivo fluorescence imaging and the antitumor efficacy of NPDC was demonstrated to be higher than that of free DOX. As such, this work convincingly demonstrates the potential of ND as a broad drug-functionalization platform.

Materials and methods

Materials and instruments

Synthetic type 1b nanodiamond powders (ND) commercially available (sizes ≈140 nm, Element Six) were chosen here because the tumor blood vessels can retain 100-400 nm particles. Then the nanodiamond powders were carboxylated[43] to use throughout the experiment. Doxorubicin hydrochloride (DOX) was purchased from Shanxi pude Pharmaceutical Co., Ltd. (China). Polyethylene glycol amine carboxyl (H_2N-PEG-COOH Mw: 2000) was bought from Shanghai seebio Biotech Inc, China. N-hydroxy succinimide (NHS), 2-(N-morphine) ethane sulfonic acid (MES) and 1- (3-dimethylaminopropyl)-3-ethyl carbodiimide hydrochloride (EDC) were purchased from Sigma. (M-β-CD) were purchased from Shanghai Aladdin Reagent Co., Ltd. (China). 3-(4, 5-dimethylthiazol-2-yl)-2, 5-diphenyltetrazolium bromide (MTT), Green streptomycin mixture and paraformaldehyde were purchased from Solarbio (Beijing, China). Dulbecco Minimum Essential Media (DMEM) was purchased from Thermo Fisher Biological and Chemical Product (Beijing, China). Fetal bovine serum was purchased from Hangzhou Sijiqing Biological Engineering Materials Co., Ltd (China). Trypsin was purchased from Sino-American Biotechnology Company. Hoechst 33258 was purchased from Beyotime Biotechnology (in China). Sucrose was purchased from Amresco Co. (USA). HeLa, HepG2 and MCF-7 cells were provided by the Gene Engineering Center of Shanxi University. All other chemicals and solvents were of analytical grade and procured from local suppliers unless otherwise mentioned. Millipore filtered water was used for all aqueous solutions.

Fluorescence spectrophotometer (970CRT, Shanghai Analytical Instruments Factory), UV-visible spectrophotometer (UV1901, Beijing spectral analysis of GM), Ultrasonic cleaner (KQ-100DE, Kunshan Ultrasonic Instrument Co., L,), High speed micro-centrifuges (TG16-W, Hunan Instrument Laboratory Instrument Development Co., Ltd.), Flip shake instrument (DR-MIX, Beijing Hao North Biotechnology Co., Ltd.), Air oscillator (THZ-22, Taicang City Experimental Equipment Factory), Fourier transform infrared spectroscopy (FTIR-8400S, Shimadzu Corporation, Kyoto, Japan), Malvern Nano Particle Sizer (ZETA Sizer, Nano-ZS90, England), Autoclave (YX280B, Shanghai Medical Devices Co., Ltd.), Transmission electron microscopy (JEM-2100, JEOL, Japan), Vacuum drying oven (DZF-6020, Shanghai Yiheng Scientific Instrument Co., Ltd.), Thermostat water bath (ZDKW-4, Beijing Zhongxing Weiye Instrument Co., Ltd.), Inverted microscope (MI11, Guangzhou Mingmei Technology Co., Ltd.), Optical microscope (XSP-8CA, Shanghai Optical Instrument Factory), Clean bench (YT-CG-1ND, Beijing Both Cologne Experiment Technology Co., Ltd.), Full automatic microplate reader (Model 550, Bio-Rad, USA), Flow cytometer (FACS Calibur, BD, USA), Laser scanning confocal microscope (Leica TCSSP5, Germany). In vivo imaging system (In-vivo xtreme, Bruker)

Preparation of ND-PEG-DOX/Na_3Cit

First, carboxylated ND is PEGylated using polyethylene glycol amine carboxyl (H_2N-PEG-COOH) and carbodiimide chemistry according to previously reported method by us.[43] Then ND-PEG was dispersed in sodium citrate (Na_3Cit, 1.0 M) medium to sonicate for 1h at room temperature followed by adding DOX and mixed thoroughly. After shaking for 6 h to make the DOX adsorb onto the ND-PEG nanoparticles exhaustively, the solution was centrifuged to remove any non-adsorbed DOX. The product, ND-PEG-DOX/Na_3Cit (NPDC), was obtained by washing three times with deionized water and finally placed in a vacuum drying oven and protected from light. The amount of DOX adsorbed was determined by calculating the change

in DOX concentration before and after the adsorption using a UV-Vis spectrophotometer at 480 nm.

Characterization of ND-PEG-DOX/ Na_3Cit

To confirm the successful synthesis of NPDC, NPDC were characterized by a Fourier transform infrared spectroscopy using KBr pellet and UV-visible spectroscopy, where both ND and ND-PEG acted as controls. Particle size, zeta potential and polydispersity index (PDI) measurements were performed in distilled water using a Zetasizer Nano ZS90. Measurements of nanoparticles size were performed at 25 °C and a scattering angle of 90°. The mean hydrodynamic diameter was determined by cumulative analysis. Determination of the zeta potential was based on electrophoretic mobility of the nanoparticles in aqueous medium, and was performed using folded capillary cells in automatic mode. The morphology of NPDC was analyzed using transmission electron microscopy.

pH-Dependent release of DOX from NPDC

The release of DOX from the NPDC in different pH was evaluated by a dialysis method. First, the same amount of complex was suspended in PBS of pH 7.4, pH 6.5 and pH 5.0 for sonication at room temperature for 30 min, respectively. Next, the suspensions were placed into dialysis bags and subsequently placed into a 50 mL centrifuge tube containing the PBS buffer solutions, respectively. The centrifuge tubes were then placed in the air oscillator maintained at 37 °C at 150 rpm. The volume of the PBS solutions in the tubes was maintained at 9 mL. At predetermined time intervals, the PBS solutions was removed and replaced with fresh medium. Dialysate was analyzed by UV-Vis spectrophotometry to determine the concentration of dissociated DOX from NPDC and the cumulative release rate.

Cell culture

HepG2 cells, HeLa cells and MCF-7 cells were cultured in a 10 cm Petri dish with a glucose Dulbecco's modified Eagle's minimal essential medium (DMEM) containing 10% fetal bovine serum (FBS) and 1% penicillin- streptomycin at 37 °C and 5% CO_2 in a humidified incubator, respectively. Cells were subcultured regularly using trypsin/EDTA.

In vitro cytotoxicity

To examine the anti-tumor effect of NPDC nanoparticles, free DOX and ND-PEG acted as a control in the experiment, respectively. The cytotoxic potential of the NPDC were assessed with an MTT assay. HepG2 cells, HeLa cells and MCF-7 cells were seeded (5×10^3cells/well) in 96-well culture plates and allowed to adhere for 16 h, respectively. Then the cells were treated with ND-PEG, NPDC or free DOX at a series of various concentrations for another 72 h. After that, treated cells were further incubated with 20μL of MTT (5 mg/mL) each well for additional 4h. The medium was then removed, and 150 μL of DMSO was added into each well for dissolution of the formazan crystals formed by living cells. After 10 min's shaking, absorbance at 490 nm was measured using a Microplate reader. Cell viability was expressed as a percentage of the absorbance to that of the control experiment without treatment. The data recorded represented the means of sixplicate measurements.

In vitro wound scratch assay

The effects on cell migration inhibition of NPDC were evaluated by in vitro scratch assay. MCF-7 cells were seeded at a density of 2×10^5 cells in each well of a 6-well plate overnight, in order to form a confluent monolayer of MCF-7 cells. Scratch wounds were made uniform shapes by manually scratching with a 10 μL pipette tip across each well and the cells were washed thrice extensively with PBS (pH 7.4) to remove cell debris and incubated at 37 °C with or without ND-PEG, NPDC and DOX. At 13 h and 27 h, the changes in the scraped areas were captured with micrographs and quantified with an imaging software system. The wound closure rate (WC) and migration inhibiting rate (MIR) was calculated by the following equation, respectively:

$$\mathrm{WC} = \left(1 - \frac{\mathrm{sw_t}}{\mathrm{sw_0}}\right) \times 100\%, \quad \mathrm{MIR} = \left(1 - \frac{\mathrm{wc_{treatment}}}{\mathrm{wc_{control}}}\right) \times 100\%$$

where SW_0 and SW_t stand for the scratch width of 0h and given time, respectively, $WC_{treatment}$ and $WC_{control}$ stand for the wound closure rate of treatment and control groups.

Cellular uptake

The cellular uptake of NPDC was visualized via a laser confocal scanning microscopy to acquire the fluorescence images of the internalized NPDC nanoparticles in MCF-7 cells, which were as a representative of investigating NPDC uptaken by cells. Briefly, MCF-7 cells at a density of 1.0×10^5 cells per dish were plated onto glass-bottomed 35mm plates in 1 mL of complete culture medium for 16 h before treatment. Next the cells were treated with the nanoparticle in culture medium (5 μg/mL of DOX equivalent) for 2 h, 5 h and 16 h, respectively. Then the medium was removed and washed thrice with ice-cold PBS. The cells were finally fixed with a 4% paraformaldehyde solution for 8 min and stained with DAPI (10 μg/mL) for 15 min to label the nucleus. The stained cells were imaged under a laser scanning confocal microscope. Samples stained with DAPI and DOX were visualized with excitation wavelengths of 405 nm and 488 nm, respectively, and the fluorescence of DOX was collected from 500 to 545 nm.

Cell uptake mechanism

To investigate the cell uptake mechanism, MCF-7 cells were seeded in a 35 mm per dish (2×10^5 cells) overnight. Then the cells were treated as follows: first, MCF-7 cells were cultured with NPDC for 2 h either at 37 °C or 4 °C. Another group of cells were cultured at 37 °C after pretreated with sodium azide (NaN_3, 0.8 M) for 30 min. Second, two pharmaco-logical inhibitors, including Methyl-beta-cyclodextrin (M-β-CD, 0.01 M) and sucrose (0.45 M) were utilized to treat MCF-7 cells for 30 min before incubation with NPDC. After culture for another 2 h, the excessive nanoparticles were removed by washing three times with PBS (pH 7.4) and the cellular uptake of NPDC was analyzed via a Flow cytometer.

Journal of Materials Chemistry B

Cell apoptosis and cell cycle

For measurement apoptosis induced by NPDC, MCF-7 cells were seeded in a 35 mm per dish and treated with the nanoparticles for 48 h. After treatment, the cells were harvested, washed twice with ice-cold PBS, stained with Annexin V-FITC and Propidium Iodide (PI) for 15 min at room temperature in the dark. The stained cells were analyzed using FACS Calibur and Cell Quest software.

The cell cycle phases can be separated into G0/G1, S andG2/M by flow cytometer analysis. To examine the effect of NPDC on the cell cycle progression, MCF-7 cells were plated at a density of 1×10^6 cells per 60 mm Petri dish in complete medium for 16–20 h. After treatment for 30 h with nanoparticles, the cells were collected and fixed with ice-cold 70% ethanol overnight at 4 °C. Thereafter, the cell pellets were treated with Propidium iodide (PI) solution containing RNase for 30 min at room temperature in the dark. Finally, the samples were analyzed by a flow cytometer. At least 10000 cells were analyzed for DNA content.

In vivo and ex-vivo fluorescence imaging

BALB/C nude mice were subcutaneously injected with HeLa cells (1×10^7 cells/mouse) in the right axilla. Fourteen days later, the tumor-bearing mice were established successfully. Then nude mice were initially anesthetized with chloral hydrate. NPDC were injected into nude mice via intraperitoneal administration at a dose of 200 μg/20 g body weight (Dox equivalent). Fluorescence snapshots of mice were acquired after administration of NPDC particles using an in vivo imaging system (In-vivo xtreme) at 0.5 h and 3.5 h. Background tissue autofluorescence was first measured by photoexcitation of the living animals at the wavelength of 480 nm with a bandwidth of 15 nm. The resulting fluorescence emission was collected at 600 nm with a bandwidth of 15 nm. Sample fluorescence imaged were taken by excitation at 480/15 nm and collection of the emission at 600/20 nm. The typical exposure time was 10 s. The acquired images were finally analyzed with the Living Image software. At 4 h post-injection, the mice were sacrificed and their organs such as liver, lung, spleen, kidneys, heart and tumor were taken out for imaging, semiquantitative biodistribution and tumor accumulation analysis using an in vivo imaging system.

In vivo antitumor efficacy

Male BALB/c-nude mice (20 ± 2 g, 6-8 weeks old) were purchased from the Chinese food and Drug Inspection Institute. All animal experiments were performed by following the protocols approved by Radiation Protection Institute of Drug Safety Evaluation Center in China (Production license: SYXK (Jin) 2013-0002). Mice were subcutaneously injected with HeLa cells (1.0×10^7cells) in the right armpit and then randomly divided into three groups (n=5) for the treatment with NPDC (100 μg of DOX equivalent per 20 g mice) or free DOX (100 μg of DOX per 20 g mice) once per 5 days by tail vein injection until the sacrifice of the animals. PBS was used as negative control. Body weight and tumor volume of mice were measured before every injection. No infection, impaired mobility, or markedly reduced food taking was observed. Tumor volume was calculated using an equation: $V = 1/2 \times a \times b^2$ mm^3, where a is the largest diameter, and b is the smallest diameter. At the end of the experiment, mice were sacrificed. Then tumors, heart, liver, spleen, lungs, and kidney were excised, weighed and photographed to evaluate therapeutic effect.

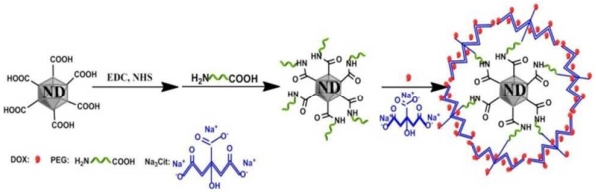

Scheme 2 The preparation of NPDC nanoparticles

Results and discussion

Preparation and characterization of ND-PEG-DOX/ Na_3Cit

The aim of this work was to design and develop high drug loading and pH-responsive drug delivery system, which delivery DOX into tumor tissue rather than normal tissue and improve the utilization rate of DOX for cancer therapy. Since PEGylated nanomaterials has been proved to enhance their solubility, permeability and stability, stimultaneously to avoid their quick recognition and elimination by the immune system, to induce prolonging the circulation in the body,[39-42] to continue to open up the application of nanodiamonds in the biology. In the present work, ND-PEG-DOX/Na_3Cit (NPDC) nanoparticles were prepared by physical adsorption DOX onto the PEGlated nanodiamond in the presence of sodium citrate, which was shown in Scheme 2. Specifically, the NPDC nanoparticles were prepared at room temperature in two steps. First, EDC and NHS were utilized as carboxyl activating regent to initiate the formation of amide linkage between carboxylated ND and H_2N-PEG-COOH, the grafting amount of PEG onto nanodiamond is 7.5×10^{-8} mol /mg (Fig. S1); in the second step, NPDC was prepared by mixing ND-PEG and DOX in the presence of 1.0 M Na_3Cit (pH 8.65), which was mainly relied on hydrogen bonds and van der Waals´forces among amines on the DOX molecules (pK_a=8.3 for DOX) and carboxylic groups on ND-PEG or Cit^{3-}.

In order to improve the amount of drug loaded onto ND-PEG nanoparticles, the adsorption of DOX onto ND-PEG vector with time was explored to obtain the absorption curve shown in Fig. 1A. One can see that the adsorption of DOX by ND-PEG nanoparticles in the sodium citrate solution quickly reached equilibrium after 6 h incubation. At the concentration of ND-PEG (1 mg/mL) and DOX (200 μg/mL), drug loading amount can reach as high as (170 ± 1.26) μg/mg by measuring the absorbance at 480 nm. This drug loading capacity is more than five times as in the deionized water (Fig. S2)[42] and more than three times as in the PB medium that of near pH value with Na_3Cit medium (pH 8.65) (Fig. S3), which demonstrated Na_3Cit plays a key role in improving the loading content of DOX.

As shown in Fig. 1A (inset), compared with the original DOX solution (right), the suspension of NPDC nanoparticles showed pale red color (left). Besides, NPDC nanoparticles illustrated rather high storage stability (Fig. S4), where the NPDC nanoparticles were

allowed to be stood at 4 °C and PBS medium (pH 7.4) for about 150 days to find the leakage rate was less than 5 %.

The formation of ND-PEG and NPDC was confirmed by Fourier transform infrared (FTIR) analysis (Fig. 1B). Compared to the spectrum of ND, in the spectrum of ND-PEG, the absorption bands at 2924 cm^{-1} is attributed to $–CH_2$ within PEG chains, which is similar to the spectrum of PEG, meanwhile, the immobilization of PEG was verified by the absorption bands at 1621 cm^{-1}, 1656 cm^{-1} and 1385 cm^{-1}, which correspond to C=O stretching, N-H bending and C-N stretching of amide bonds, indicating that PEG was indeed conjugated to the surface of ND. In the NPDC, the absorption bands that marked in redlining box confirmed the existence of Na_3Cit in NPDC, which could be supported with redlining box in the Na_3Cit, the adsorption band at 1409 cm^{-1} corresponding to the phenyl ring vibration of DOX moiety, which is in consistent with FTIR spectrum of DOX as black arrow indicated. The results suggested that DOX and Na_3Cit were successfully attached on the surface of ND-PEG.

Although the reddish color of the NPDC suspension indicated the presence of DOX (Fig. 1A inset), NPDC was further characterized by UV-Vis absorption. The spectrum of DOX, ND, ND-PEG and NPDC are shown in Fig. 1C. NPDC displayed the same absorption band like free DOX at 480 nm, which demonstrated that DOX moiety was absorbed on ND-PEG.

Transmission electron microscopy (TEM) was used to further verify the formation of the intermediates and NPDC complex. Fig. 1D shows the typical images that before and after coating with different molecules. Clear structures were visible in samples of ND and ND-PEG, the structures of ND were markedly less visible after the formation of NPDC. It can be obviously seen that NPDC was different from the first two materials, where single ND particle was hardly found and some pellets were formed, implying that the DOX coated on the surface of ND-PEG by favor hydrogen bonds and van der Walls´ forces. Approximately spherical DOX was attributed to the presence of sodium citrate, which is also proved by free drug in sodium citrate media (Fig. S5).

In addition, various factors can affect the successful application of a nanoscale-drug delivery platform in the clinic, for example, drug size and surface charge have an effect on blood circulation,

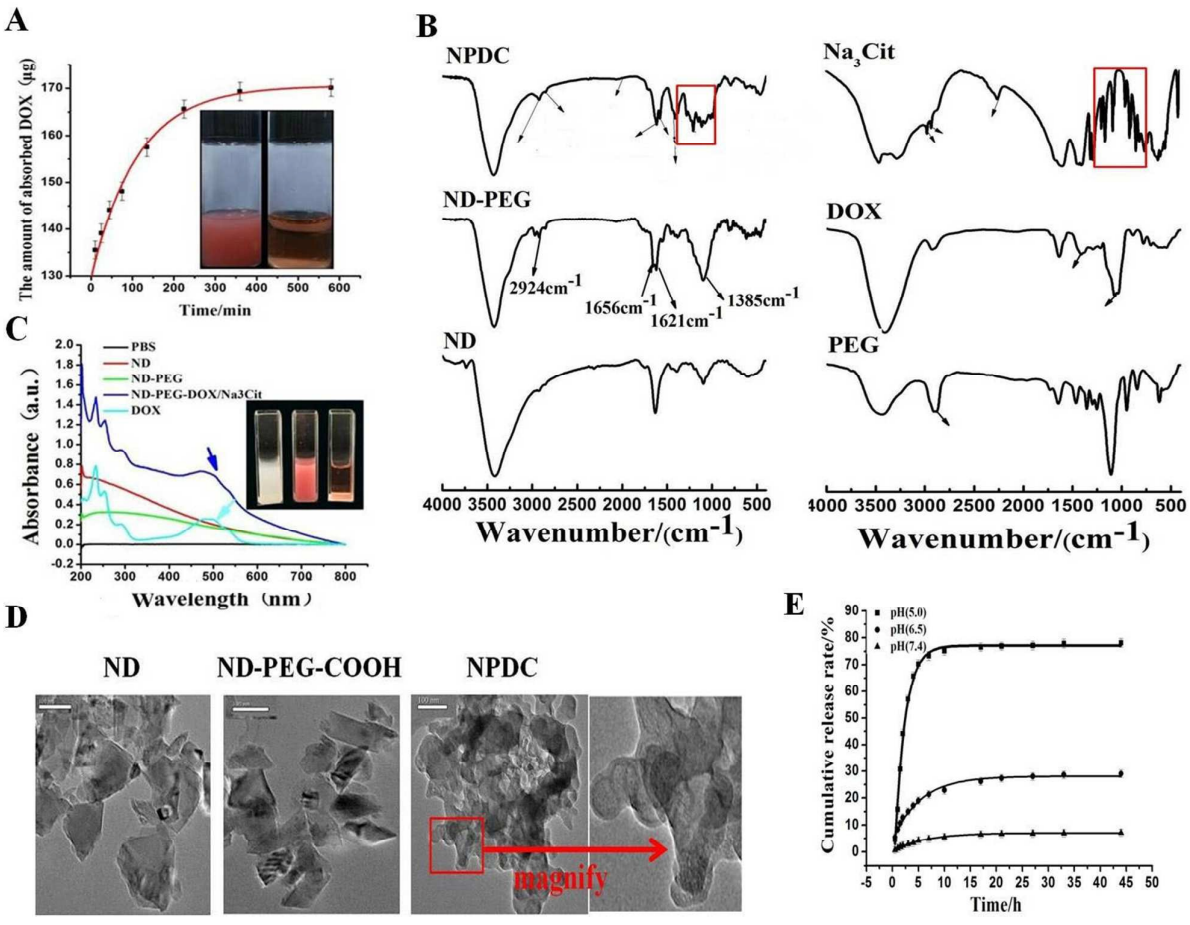

Fig. 1 Characterization and in vitro drug release properties of NPDC. (A) Adsorption of DOX onto PEGylated ND in sodium citrate solution (1.0 M) with time. (Inset: the DOX solution before (right) and after (left) adsorbed by ND nanoparticles, the concentration of DOX is 200 μg/mL.). (B) FTIR Spectra of various materials. (C) UV-Vis absorption of DOX, ND, ND-PEG and NPDC in PBS. (Inset: The photographs in the PBS solutions of ND-PEG, NPDC and DOX in left-to-right order). (D) Typical

Journal of Materials Chemistry B

transmission electron microscopic images before and after coating with different molecules, respectively. The scale bars represent 100nm. (E) In vitro drug release profiles of NPDC at 5.0 ( ), 6.5 ( ), 7.4 ( ).

Table. 1 Particle size, Zeta potential and PDI of ND, ND-PEG and NPDC

	Diameter (nm)	Zeta potential (mv)	PDI
ND	166.0±1.6	-30.2±1.0	0.164
ND-PEG	184.6±6.4	-24.7±1.9	0.126
NPDC	210.5±4.5	-27.8±1.6	0.079

tissue distribution, clearance and passive targeting to tumor sites, so particle size and zeta-potential analysis were applied to ND-PEG and NPDC complexes by dynamic light scattering (Seen Table.1). Seen from Table. 1, the pristine ND possessed an average size nearly 166 nm with a PDI of 0.164, while the zeta potential analysis showed that the surface of ND was negative charged with an average particle value of -30.2 ± 1.0 mV. After conjugating PEG to ND, the zeta potential showed increased negative potential of -24.7 ± 1.9 mV, and the increased size 184.6 ± 6.4 nm with a PDI of 0.126. An increase in nanoparticle size after PEGylation could be attributed to the stretch of PEG chains on the PEGylated ND surface. Moreover, the zata potential of ND-PEG was a little higher than that of ND, which might primarily result from the reduced carboxyl groups due to the barrier shield effect of PEG chains on the ND. Compared to ND-PEG, the NPDC exhibited a lower negative surface charge of -27.8 ± 1.6 mV, which might be attribute to the existence of carboxylic acid groups on Na_3Cit, and NPDC had a larger size of 210.5 ± 4.5 nm with a PDI of 0.079, which could greatly benefit the aggregation in tumor site because of the well-known enhanced permeability and retention (EPR) effect that the tumor blood vessels can retain 100-400 nm particles.[44] Compared to the pristine NDs, the PDI of ND-PEG and NPDC were decreased gradually, which indicated that the dispersity of nanoaprticles was improved accordingly. Thus, the dimension and well dispersibility of NPDC was very suitable for drug delivery.

The effect of pH on DOX release from ND-PEG-DOX/Na_3Cit

For the successful application of ND as a drug delivery platform, it is important that specific and sustained drug release occur only upon reaching the target site. Premature release of DOX will induce toxicity in the blood circulatory system, such as damage to normal cells, tissues or metabolic breakdown. Since the nanoparticles may interact with cells in the body, where the pH ranges from 7.4 to 4.5, drug release from nanoparticles by environment pH stimuli is prerequisite to result in minimizing toxicity toward normal tissue. Here the drug release from NPDC was carried out at 37 °C in the PBS buffer of pH 5.0, 6.5 and 7.4. As shown in Fig. 1E, the rate and amount of DOX released from NPDC were dependent on the pH of the medium. About only 7 % of DOX were released even if NPDC released lasted 50 h at pH 7.4, it was greatly decreased five folds compared to the previous report.[42] However, the amount of DOX released increased with pH values decreased, at pH 6.5 (a simulated tumor environment), NPDC released about 25 %. When the pH was decreased to 5.0, the released DOX was markedly increased nearly 80 %, which is about twice as high as the previous work,[43-45] as it was expected that the NPDC nanoparticles had minimal drug release (under simulated physiological conditions, pH 7.4), but much more DOX were released in acidic endosomes of cells (pH 5.0-5.5). This pH-responsive release property can be chiefly associated with the hydrogen bonds damage between amino of DOX and carboxy of Cit^{3-}, which is influenced by pH. According to the previous work,[45] the release of unmodified DOX achieved 54 % at pH 7.4; in comparison with NPDC, free DOX can damage cells in a normal physiological environment, causing serious side effects. The results suggested the NPDC drug delivery system has potential applications for controlled drug release.

Cytotoxicity assay

Considering the high drug-loading efficiency and pH adjustable release drug, NPDC nanoparticles might be a promising drug delivery system for cancer therapy. Here, .the cytotoxicity effect was examined using an MTT assay, where HepG2, HeLa and MCF-7 cells were selected to determine the effect on cell proliferation. Cells were first incubated with NPDC for 72 h with various concentrations of DOX, and their relative cell viabilities are shown in Fig. 2. Both free DOX and NPDC were found to inhibit cell proliferation, and the relative cell viability declined monotonously with ascending the concentration of DOX. When the concentration of DOX was very low (1 μg/mL), both NPDC and free DOX had similar cytotoxic effects on both HepG2 and MCF-7cells. However, NPDC obviously showed a higher cytotoxic effect on both cells than that of free DOX in increasing the concentration of DOX. For example, the viability of HepG2 cells was 20 % for NPDC and 30 % for free DOX with 3 μg/mL DOX. Meanwhile, the MCF-7 cells viability was only 8 % for NPDC and 15 % for free DOX at the same concentration of DOX. The MTT assay implied that MCF-7 cells were the most sensitive to NPDC, which exhibited the highest cytotoxicity among the three cell lines in the same conditions. Furthermore, it was worthy note that NPDC with a low concentration behaved similar cytotoxicity to free DOX with a high concentration. For instance, the viability for HepG2 cells was 24 % at free 9 μg/mL DOX, while it was 20 % for NPDC at 3 μg/mL, which indicated NPDC nanoparticles can significantly improve the drug efficacy.

In addition, the cytotoxicity of both NPDC and free DOX with incubation time was also investigated (Fig. S6). The result displayed that NPDC has a slowly release drug ability and a higher anticancer activity than that of free DOX with time prolonging. Besides, there was no noticeable difference in cell viability both the ND-PEG groups and the control groups, which showed that the ND-PEG has a good biocompatibility.

Moreover, we investigated the effects of free DOX, ND-PEG and NPDC on cellular morphologies (Fig. S7) with time. Morphological

changes of the three cells treated with free DOX and NPDC have similar results with the cell viability.

In wound scratch assay

To determine cell migration, the scratch assay was performed in the presence of NPDC (5 μg/mL of DOX equivalent). As shown in Fig. 3A, the scratch width is evidently narrowed while MCF-7cells treated by ND-PEG even if time increases, which is similar to the control group. However the scratch width is nearly essentially unchanged while MCF-7 cells were treated with NPDC and DOX, the migration inhibiting rate of NPDC and DOX were up to 87.35 % and 82.32 % in Fig. 3B, respectively. Therefore, the NPDC can inhibit cell migration effectively.

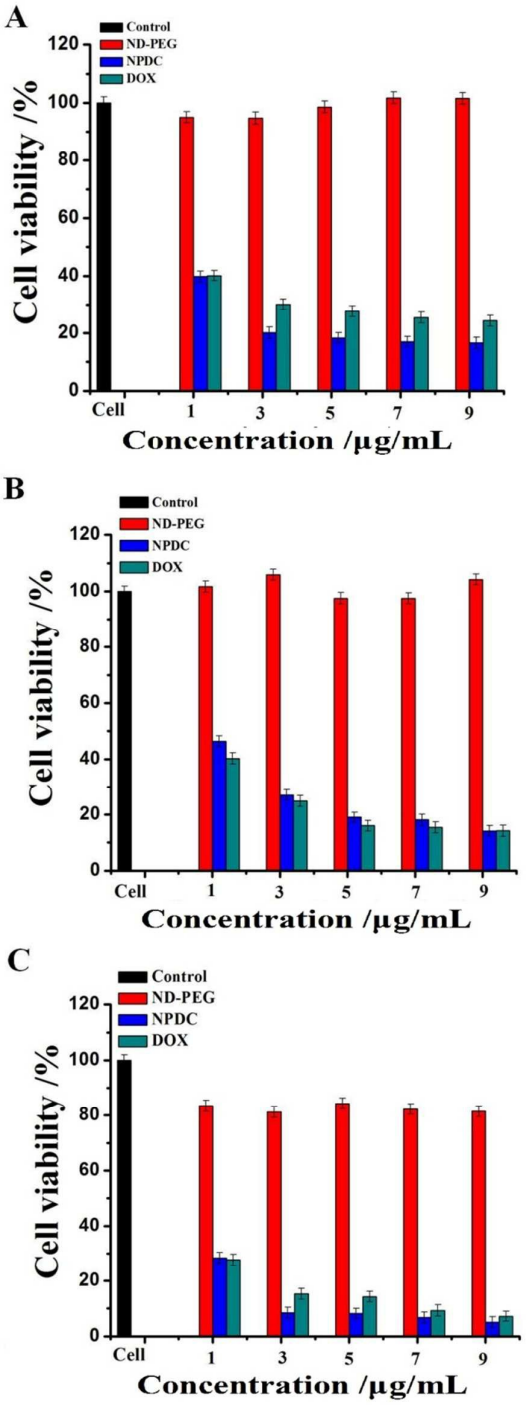

Fig. 2 Effect of free DOX and NPDC on HepG2, HeLa and MCF-7 cell viability for 72h was measured by MTT assay. (A) HepG2 cells, (B) HeLa cells and (C) MCF-7 cells. Experiments were repeated three times and data are presented as the mean ± SD (for each group, n = 6).

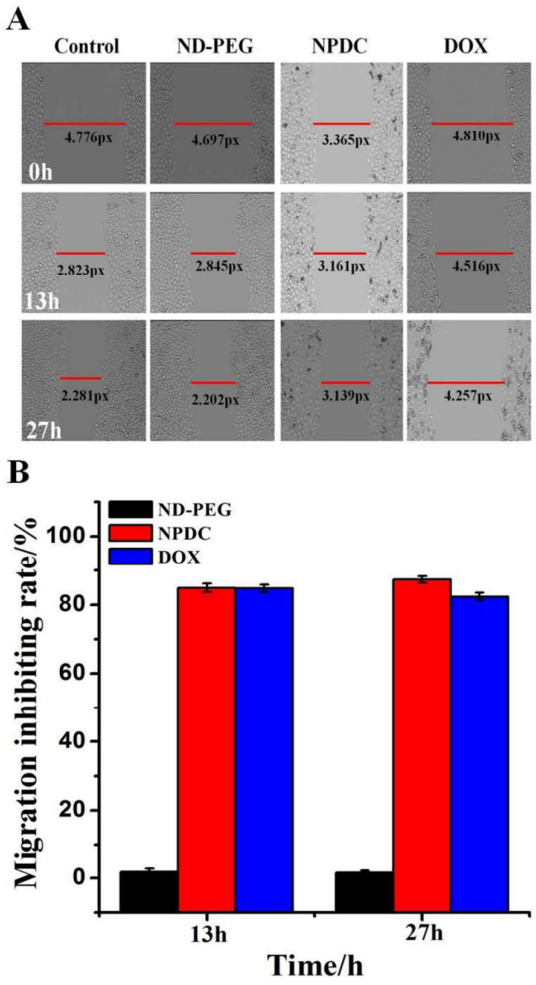

Fig. 3 Effect of free DOX and NPDC on MCF-7 cells migration inhibition by wound scratch assay with time. (A) Representative images of MCF-7 cells treatment by NPDC and free DOX, MCF-7 cells untreated as controls. (B) The plot was obtained by migration inhibiting rate vs. time, where data were adopted from Fig. 3A.

Intracellular accumulation and cellular uptake mechanism

Although the NPDC nanoparticles were found to be active, whether they have entered the cells or remained in the extracellular fluid

was still unknown. Moreover, the therapeutic effect of DOX was dependent on its ability to inhibit the synthesis of nucleic acid through intercalation after entrance into nucleus. Therefore, to study whether the nanoparticles can enter living cells and DOX dissociated from NPDC nanoparticles, we used laser scanning confocal microscopy to record and examine the images of the distribution of nanoparticles in the cells. In the experiment, using MCF-7 cells as a model, the cells were treated by NPDC with 5 μg/mL of DOX equivalent for 2 h, 5 h and 16 h, respectively, or treated with free DOX (5 μg/mL) for 1 h. Then cells were subjected to nuclear staining, followed by laser scanning confocal microscopy with excitation wavelength of 488 nm and emission wavelength at 560-590 nm. As shown in Fig. 4A, free DOX quickly entered into the cells and located in the cell nucleus after treatment for 1 h due to small molecule rapidly diffusion into the cell. In Fig. 4B, the green fluorescence signal of DOX from NPDC was distinctly observed in the cytoplasm alone after treatment with NPDC for 2 h and 5 h, but green fluorescence signal enhancement was seen at 5 h. When the incubation time was extended to 16 h, the green fluorescence was found both in the cytoplasm and nucleus, but were mainly exhibited much accumulation in the nucleus. Such a result implied that NPDC moved inside the cells and were capable of delivering the drug inside living cells efficiently. Then DOX molecules were detached from the NPDC and followed migrating into the nucleus. This would lead to a sustained functional drug release compared to free DOX, which is consistent with the gradual DOX release from NPDC complexes in PBS at 37 °C (Fig. 1E). The result was also accordant with the previous report by us,[18,42,45] which indicated the potential applications of NPDC for controlled drug delivery.

Due to the fact that side scatter (SS) by flow cytometry analysis can indicate the particle complexities within the cells, the cellular uptake of NPDC can be indirectly demonstrated by SS. Fig. 4C showed that the SS of NPDC uptake by MCF-7 cells after 1 h and 7 h incubation, respectively. After coculture with NPDC for 1 h, the value of SS only slightly increased, but it greatly increased after incubation 7 h. The result suggests that the NPDC nanoparticles indeed enter the cells and the cell uptake is a time-dependent process.

To further examine the uptake kinetics of NPDC in cancer cells, MCF-7 cells were treated with the same concentrations of NPDC for different time and analyzed by flow cytometer. As shown in Fig. S8, the cellular uptakes of NPDC and free DOX were greatly strengthened with time increased and the fluorescence intensity reached a plateau at about 7 h for NPDC and 3 h for free DOX. Curve fitting by single exponent function showed that the rate constants (k) of the endocytosis for NPDC was about 0.239 h^{-1}, namely, the value of uptake half-life was near 2.90 h, while the value of uptake half-life of free DOX was about 0.93 h, which indicated that the uptake rate of NPDC was approximately three times slower than free DOX. However, after 6 h, the uptake of the NPDC nanoparticles significantly improved (Fig. S7). These results are related to cellular uptake pathways. The uptake of DOX occurs through an energy-independent passive diffusion mechanism,[18] while the NPDC nanoparticles can efficiently delivery the drug inside living cells via both clathrin- and caveolae-dependent endocytosis pathway (Fig. 4D).

We further evaluated the mechanism of uptake of NPDC nanoparticles. In these experiments, first, the NPDC were incubated with the cells at either low temperature (4 °C instead of 37 °C) or in ATP-depleted environments (cells pretreated with sodium azide, NaN_3). Sodium azide is an agent that blocks the formation of adenosine 5- triphosphate (ATP) within cells.[46-47] While the energy metabolism of cells maintains at a low level at 4 °C, this was the case that a decrease in the uptake of the NPDC was observed. The cellular uptake either treated with sodium azide or low temperature of 4 °C was 90 % and 64 % inhibition, respectively (Fig. 4D). The results directly indicate that the cell uptake of NPDC

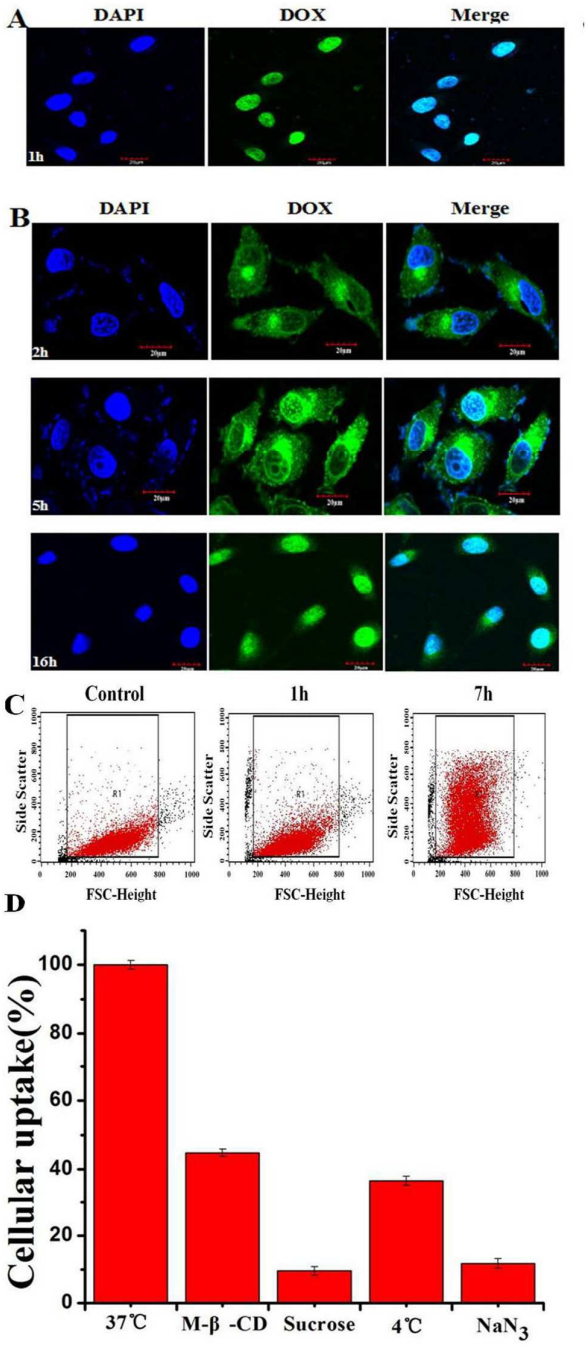

Fig. 4 Cellular uptake, distribution and uptake mechanism of NPDC nanoparticles. (A)Confocal laser scanning microscopy (CLSM) images of MCF-7 cells treated with free DOX for 1h. (B) Confocal laser scanning microscopy (CLSM) images of MCF-7 cells treated with NPDC in 2h, 5h and 16h, respectively. The images (A-B) in the left column show the cell nucleus dyed with DAPI; the middle column shows DOX fluorescence, and the right column shows the merge of the two previous images. (C) The variations of side scatter (SS) after MCF-7 cells were treated with NPDC for 1h and 7h was quantified from a minimum of 10000 cells by Cell Quest software using flow cytometry analysis, respectively. Y-axis is side scatter (SS), which indicated intracellular particle complexity; X-axis is forward scatter (FSC). (D) Quantitative analysis of mechanistic study of the uptake of NPDC under different treatment conditions.

system was an energy and temperature-dependent process. Next, we determined whether the uptake was likely due to a clathrin- or caveolae- mediated process. The following studies were carried out: cells were pretreated with either sucrose or M-β-CD medium. Sucrose is known to disrupt the formation of clathrin coated vesicles and M-β-CD is known as damage for cholestero composition on cell membrane. In the presence of sucrose pretreat-ment showed drastically lower uptake (only by 9 %). Similar steps were taken to evaluate the contribution of caveolae- mediated endocytosis by treating cells with M-β-CD (10 mmol), led to around 55 % reduction in cell uptake. The results indicate that the internalization of NPDC goes through both clathrin- and caveolae-dependence, but the clathrin performance is more prominent than that caveolae-dependence. This is due to the presence of spherical doxorubicin. To our knowledge, the nanodiamond carriers for DOX loaded as moleculars were clathrin-mediated process,[18,33,42,43,45] while the NPDC system was found to be both clathrin- and caveolae mediated process, suggesting that there is a link between uptake mechanism and shape of DOX onto the surface of ND. Our finding is in agreement with previous report that chan and their coworkers demonstrated the relation between the mechanism of cellular uptake and different sizes and shapes for nanoparticles.[48]

Cell apoptosis and cell cycle

The effect of ND-PEG, NPDC and DOX on cell apoptosis was as

Journal of
Materials Chemistry B

ARTICLE

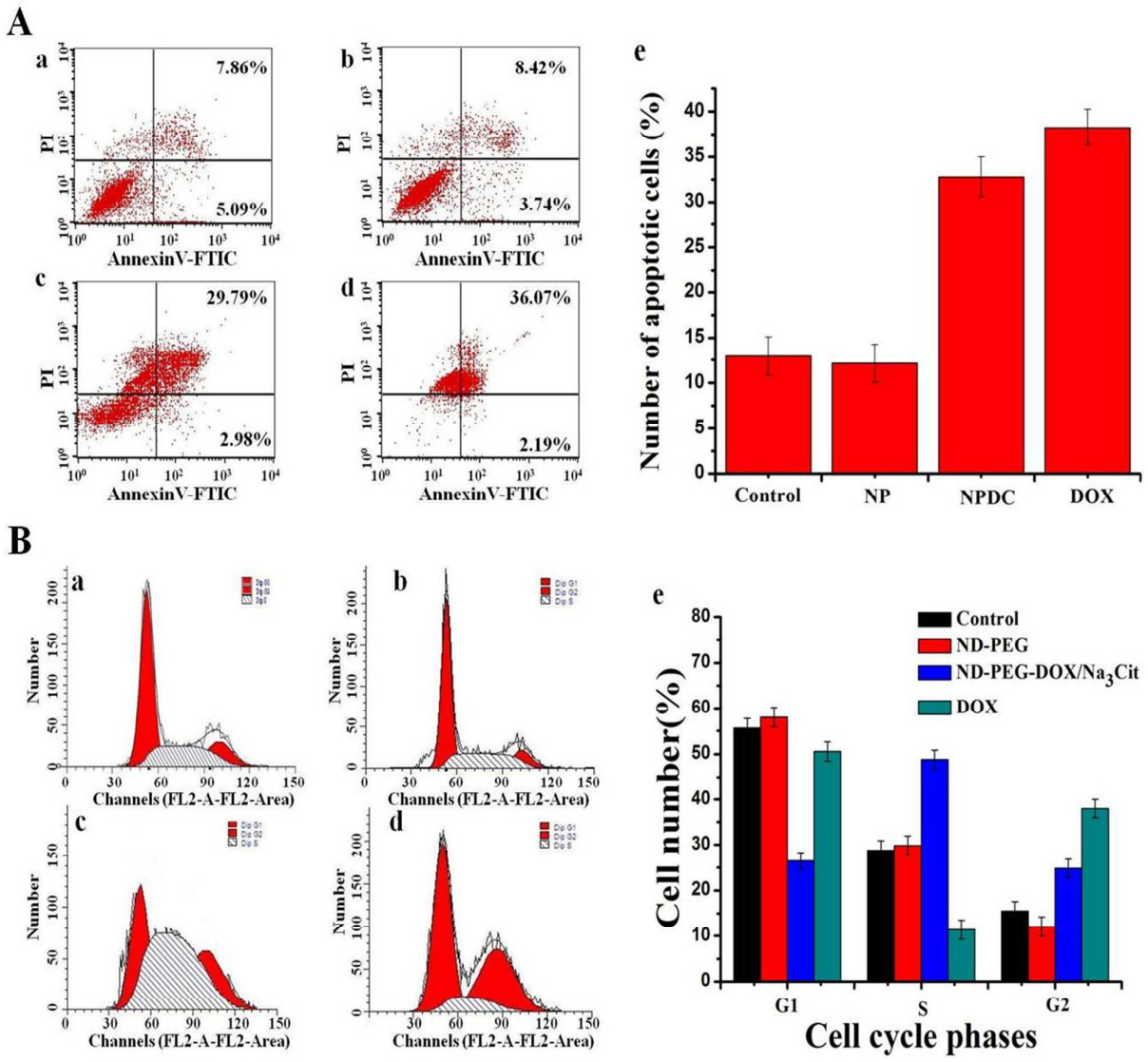

Fig. 5 Flow cytometry analysis. (A) Apoptosis of MCF-7 cells induced by ND-PEG (b), NPDC (c) and DOX (d) for 48h, MCF-7 cells untreated as control (a), the number of apoptotic cells (e), where date were adopted from a,b,c and d. (B) Cell cycle of MCF-7 cells induced by ND-PEG (b), NPDC (c) and DOX (d), MCF-7 cells untreated as control (a), the cell cycle histogram (e), where data were adopted from a,b,c and d.

well investigated. In the apoptosis quadrant diagram, each represents that the living cells, early apoptosis cells, late apoptosis cells and debris cells in a counter clockwise direction from the left bottom. As observed from the morphology of NPDC to cancer cells, free DOX and NPDC could induce cell apoptosis, after treatment for 48 h (Fig. S7). The apoptotic cells were further quantified using prodium iodide (PI)/Annexin V staining by flow cytometric analysis (Fig. 5A). In Fig. 5A (b), the cells treated with ND-PEG displayed similar to the cells untreated, it could not induce cell apoptosis, implying that ND-PEG was nontoxic. While about 33 % cell

apoptosis was induced by NPDC (Fig. 5A(c)) and a little lower compared to that induced by free DOX (38 %) (Fig. 5A(d)). The results again confirmed that DOX could efficiently release from NPDC in cells and resulted in cell apoptosis, and that mainly induced late cells apoptosis, which is consistent with free DOX.

DOX could insert into the minor grooves of nucleic acids to inhibit their synthesis, and finally change the cell cycle.[49] Fig. 5B showed that cells treated with ND-PEG exhibited similar cell cycle with control cells, while NPDC (Fig. 5B(c)) and free DOX (Fig. 5B (d)) significantly changed the cell cycle, resulting in 29.19 % and 5.06 % reduction in the percentage of G0/G1 phase, 9.21 % and 22.44 % increase in the percentage of G2/M phase, respectively. From Fig. 5B (e), we can see that the cells treated with NPDC increased at the percentage of S phase, which implied that NPDC can change the cell cycle and mainly block in S phase, while the group treated with free DOX was blocked in G2/M phase. The results showed that both NPDC and free DOX emerged different cell cycle blocking and the difference is attributed to different intracellular distributions for them.

In vivo and ex-vivo fluorescence imaging and biodistribution

In vivo imaging was used to investigate the in vivo targeting of NPDC. Fig. S9 gave the fluorescence signal and intensity distribution as a function of time for the NPDC delivered systemically via intraperitoneal injections. Stronger signals of the NPDC were visualized in the mouse after 0.5 h. More importantly, the stronger signal was observed in tumor site after 3.5 h, which indicated that the NPDC can be targeted in the tumor site. To further determine NPDC in vivo biodistribution, at 4 h after intraperitoneal administration with NPDC, the tumor-bearing mice were sacrificed, and the heart, liver, spleen, lung, kidney and tumor were excised. The distribution of NPDC in each tissue was observed by means of fluorescence of DOX from NPDC using xtreme in vivo imaging system. As displayed in Fig. 6A, in the organs and tumors of tumor-bearing mice treated with PBS, there is ignorable autofluorescence from hemeproteins, while NPDC showed relatively high fluorescence intensity from DOX in tumor and low fluorescence intensity in the heart, liver, spleen, lung, kidney (Fig. 6B). The mean fluorescence of organs and tumors analyzed by region-of-interest (ROI) was displayed on Fig. 6C, where data come from Fig. 6A and Fig. 6B, showing that the NPDC were mainly accumulated in tumor site. Specifically, the content of NPDC in tumor was about 2-3-fold that of other organs, likely due to the enhanced permeability and retention (EPR) effect.[50-51] The high tumor accumulation of NPDC would enhance their antitumor effect in vivo.

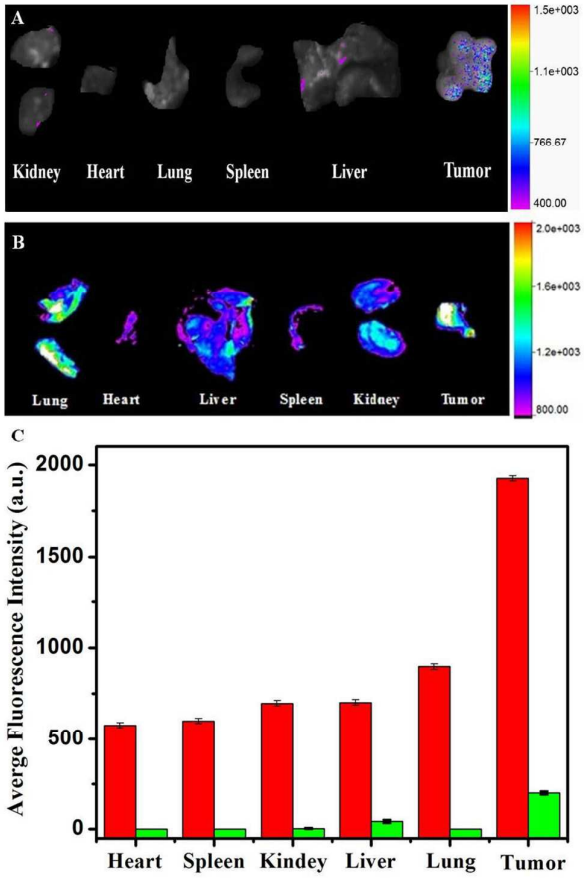

Fig. 6 Ex vivo images of NPDC in nude mice after intraperitoneal injection. (A) Ex vivo fluorescence images of the extracted tumor and organs that treated with PBS. (B) Ex vivo fluorescence images of the extracted tumor and organs that treated with NPDC. The color bars correspond to the detected fluorescence intensity. (C) The plot was obtained by average fluorescence intensities vs. tumor and organs, where data come from Fig. 6A and Fig. 6B.

In vivo antitumor efficacy

To assess the effect of NPDC on tumor growth, HeLa tumor-bearing mice were treated with NPDC, free DOX (100 μg of DOX equivalent per 20 g mice), and PBS, respectively. As shown in Fig. 7B, both NPDC and DOX exhibited significant tumor inhibition, whereas the tumor grew rapidly in the control group treated with PBS. Excitingly, inhibition of NPDC was markedly more than that of free DOX. On day 25 after treatment, NPDC and free DOX inhibited tumor growth by 78.9 ± 2.63 % and 28.0 ± 7.06 %, respectively (Fig. 7C and 7D). Such a result indicated that NPDC has an excellent antitumor effect. Besides, it is worth noting that there was a significant loss in weight of mice after DOX treatment compared to PBS groups, while NPDC-treated groups exhibited weight gain with time increasing (Fig. 7A). Furthermore, organ indices were also measured at this experiment, which provide information on the general toxicity. The organ indices were defined as the ratio of the wet weight of the organ to the whole body weight (g/g). The decrease of the organ indices

Journal of Materials Chemistry B

means organ shrinking or function weakening, while the increase usually means that the organ is congested, swelled, proliferated or function is strengthened.[33] A typical set data for the measurement was shown in Fig. 7E. There is no apparent difference in the heart, liver, lung and kidney indices of NPDC and control groups, indicating that multiple injections of the NPDC do not cause obvious toxic effects. But a significant difference was observed in the liver, lung and spleen indices of in DOX group compared to control group. In addition, both NPDC and DOX groups have toxicity on spleen, but compared with the PBS group, significantly reduced side effects. Hence such a founding entailed NPDC nanomedicine significantly low toxicity compared with that of DOX. In addition, no abnormal clinical signs or behaviors were detected in either PBS groups or experimental groups during the entire course of the study. Taken together, these results corroborate the suggestion that the NPDC administration does not induce any apparent toxicity in mice during the study period, which verified powerfully the superior tumor target ability of NPDC, as predicted via in vivo and ex-vivo fluorescence imaging. Thus, NPDC displayed enhancing antitumor efficacy with low toxicity through high drug loading capacity, pH-responsive drug release and enriching accumulation in tumor site.

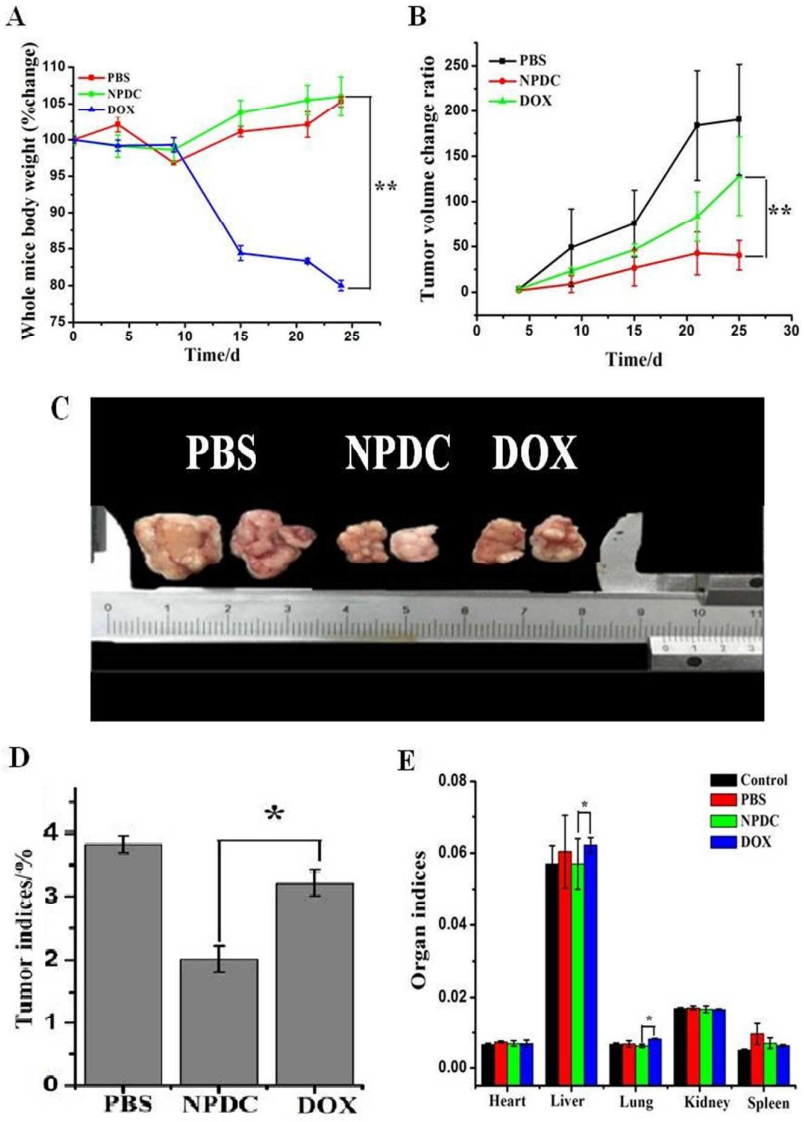

Fig. 7 In vivo biological effect for NPDC and DOX, in which PBS as a control. (A) Average whole mice weight analysis of tumor-bearing mice treated with PBS (n = 5), NPDC (100 μg of DOX equivalent per 20 g mice) (n = 5) or DOX (100 μg /20 g mice) (n = 5) via tail intravenous injections every 5 days. (B) Average tumor volume change analysis for mice treated with PBS (n = 5), NPDC (100 μg of DOX equivalent per 20 g mice) (n = 5) and DOX (100 μg /20 g mice) (n = 5) via tail intravenous injections every 5 days. (C) Representative images of tumors from treated mice for 25 days. (D) Tumor indices of PBS-injected (n = 5), NPDC-injected mice (n = 5) and DOX (n = 5) on day 25. (E) Comparison of the organ indices of PBS-injected (n = 5), NPDC-injected mice (n = 5) and DOX (n = 5), where nude mice missed tumors served as a control group (n = 3). Data are represented as means ± SD.

Conclusions

In this work, we investigated augmented anticancer activity of nanomedicine based on PEGylated nanodiamond. Initially, we fabricated a NPDC drug delivery system with high DOX loading in sodium citrate medium, which plays a key role in adsorption and dissociation of DOX. Simultaneously, the NPDC system exhibited excellent physiological stability and pH controlled drug release with high cytotoxicity to cancer cells compared to free drug. The results showed that the NPDC system was taken up into the cells via both clathrin- and caveolae-mediated endocytosis process, which is first found in nanodoiamond as a carrier. We proposed the phenomenon related to shapes of drug onto the surface of ND. Furthermore, NPDC showed a more and slower uptake in comparison to free drug. What is more, flow cytometer and confocal microscope analysis proved that NPDC can easily pass into cells and constantly sustained releasing DOX to nucleus, which indicated that NPDC can prolong the circulation time of anticancer drug and improve the antitumor activity. It was also illustrated that NPDC can inhibit the cell migration. Besides, we obtained that NPDC induced cell apoptosis, which is mainly late apoptosis-dependent, and NPDC can change the cell cycle. Finally, in vivo biological effect demonstrated that NPDC chiefly accumulated in the tumor site and enhanced antitumor efficiency with low toxicity beyond conventional DOX treatment. This simple, efficient, and flexible strategy led to a promising targeted and controlled drug release system for potential clinical application and would assist in the further design and develop biomedical application of smart nanoparticles.

Acknowledgements

This work is supported by the National Natural Science Foundation of China (Grant No. 21071091), Shanxi Science and Technology Development Program (Grant No. 20130313021-1).

Notes and references

1 Y. L. Wu, H. L. Zhang and Y. M. Yang, *Drug. Discov. Today.,* 2015, **20**, 766.
2 R. S. Zheng, X. X. Peng, H. M. Zeng, S. W. Zhang, T. H. Chen, H. M. Wang and W. Q. Chen, *Cancer. Lett.,* 2015, **363**, 176.
3 M. Das, S. R. Datir, R. P. Singh and S. Jain, *Mol. Pharm.,* 2013, **10**, 2543.
4 X. M. Wu, X. R. Sun, Z. Q. Guo, J. B. Tang, Y. Q. Shen, T. D. James, H. Tian and W. H. Zhu, *J. Am. Chem. Soc.,* 2014, **136**, 3579.
5 Y. K. Lee, J. Choi, W. P. Wang, S. Y. Lee, T. H. Nam, W. S. Choi, C. J. Kim, J. K. Lee, S. H. Kim, S. S. Kang and D. W. Khang, *ACS Nano.,* 2013, **7**, 8484.
6 P. Mohan and N. Rapoport, *Mol. Pharm.,* 2010, **7**, 1959.
7 S. Licata, A. Saponiero, A. Mordente and G. Minotti, *Chem. Res. Toxicol.,* 2000, **13**, 414.
8 X. R. Li, X. C. Yang, Z. Q. Lin, D. Wang, D. Mei, B. He, X. Y. Wang, X. Q. Wang, Q. Zhang and W. Gao, *Eur. J. Pharm. Sci.,* 2015, **76**, 95.
9 Z. S. Ge and S. Y. Liu, *Chem. Soc. Rev.,* 2013, **42**, 7289.
10 V. R. N, S. R. Mane, A. Kishore, J. D. Sarma and R. Shunmugam, *Biomacromolecules.,* 2012, **13**, 221.
11 J. Q. Fan, G. Fang, F. Zeng, X. D. Wang and S. Z. Wu, *Small.,* 2013, **4**, 613.
12 L. Moore, E. K. H. Chow, E. Osawa, J. M. Bishop and D. Ho, *Adv. Mater.,* 2013, **25**, 3532.
13 X. Q. Zhang, R. Lam, X. Y. Xu, E. K. Chow, H. J. Kim and D. Ho, *Adv. Mater.,* 2011, **23**, 4770.
14 J. Li, Y. Zhu, W. X. Li, X. Y. Zhang, Y. Peng and Q. Huang, *Biomaterials.,* 2010, **31**, 8410.
15 E. K. Chow, X. Q. Zhang, M. Chen, R. Lam, E. Robinson, H. J. Huang, D. Schaffer, E. Osawa, A. Goga and D. Ho, *Sci. Transl. Med.,* 2011, **3**, 73.
16 P. Villalba, M. K. Rama, H. Gomez, V. Bhethanabotlae, M. N. Helms, A. Kumar and A. Kumar, *Mater. Sci. Eng. C.,* 2012, **32**, 594.
17 J. S. Xiao, X. P. Duan, Q. Yin, Z. W. Zhang, H. J. Yu and Y. P. Li, *Biomaterials.,* 2013, **34**, 9648.
18 Y. Q. Li, X. P. Zhou, D. X. Wang, B. S. Yang and P. Yang, *J. Mater. Chem.,* 2011, **21**, 16406.
19 N. Mohan, C. S. Chen, H. H. Hsieh, Y. C. Wu and H. C. Chang, *Nano Lett.,* 2010, **10**, 3692.
20 V. Vaijayanthimalaa, P. Y. Cheng, S. H. Yeh, K. K. Liu, C. H. Hsiao, J. I. Chao and H. C. Chang, *Biomaterials.,* 2012, **33**, 7794.
21 A. M. Schrand, S. A. C. Hens and O. A. Shenderova, *Crit. Rev. Solid State Mater. Sci.,* 2009, **34**, 18.
22 Y. Yuan, X. Wang, G. Jia, J. H. Liu, T. C. Wang, Y. Q. Gu, S. T. Yang, S. Zhen, H. F. Wang and Y. F. Liu, *Diam. Relat. Mater.,* 2010, **19**, 291.
23 X. Y. Zhang, J. L. Yin, C. Kang, J. Li, Y. Zhu, W. X. Li, Q. Huang and Z. Y. Zhu, *Toxicol. Lett.,* 2010, **198**, 237.
24 H. Schwertfeger, A. A. Fokin and P. R. Schreiner, *Angew. Chem. Int. Ed.,* 2008, **47**,1022.
25 Q. W. Zhang, V. N. Mochalin, I. Neitzel, I. Y. Knoke, J. J. Han, C. A. Klug, J. G. Zhou, P. I. Lelkes and Y. Gogotsi, *Biomaterials.,* 2011, 32, 87.
26 I. Neitzel, V. Mochalin, I. Knokc, G. R. Palmese and Y. Gogotsi, *Compos. Sci. Technol.,* 2011, **71**, 710.
27 Q. W. Zhang, V. N. Mochalin, I. Neitzel, K. Hazeli, J. J. Niu, A. Kontsos, J. G. Zhou, P. I. Lelkes and Y. Gogotsi, *Biomaterials.,* 2012, **33**, 5067.
28 J. Tisler, R. Reuter, A. Lammle, F. Jelezko, G. Balasubramanian, P. R. Hemmer, F. Reinhard and J. Wrachtrup, *ACS Nano.,* 2011, **5**, 7893.
29 J. C. Arnault, T. Petit, H. Girard, A. Chavanne, C. Gesset, M. Sennour and M. Chaigneau, *Phys. Chem. Chem. Phys.,* 2011, **13**, 11481.
30 V. N. Mochalin, O. Shenderova, D. Ho and Y. Gogotsi, *Nature Nanotech.,* 2012, **7**, 11.
31 P. C. Tsai, O. Y Chen, Y. K. Tzeng, Y. Y Hui, J. Y Guo, C. C. Wu, M. S. Chang and H. C Chang, *EPJ. Quantum. Technology.,* 2015, **2**, 1.
32 A. Pentecost, S. Gour, V. Mochalin, I. Knoke and Y. Gogotsi, *ACS. Appl. Mater. Interfaces.,* 2010, **2**, 3289.
33 Z. Q. Wang, Z. M. Tian, Y. Dong, L. Li, L. Tian, Y. Q. Li and B. S. Yang, *Diam. Relat. Mater.,* 2015, **58**, 84.
34 P. F. Liu, W. J. Gao, Q. S. Zhang, K. Chen, J. Zhang, L. Chen, X. Y. Zhang and K. Wang, *React. Funct. Polym.,* 2015, **89**, 1.
35 E. Zhang, A. D. Kosinska, Z. Y. Ma, K. K. Dietze, Y. Xu, Z. J. Meng, X. Y. Zhang, J. Z. Wang, B. J. Wang, U. Dittmer, M. Roggendorf, D. L. Yang and M. J. Lu, *Virology.,* 2015, **475**, 56.
36 L. Zhao, Y. H. Xu, T. Akasaka, S. Abe, N. Komatsu, F. Watari and X. Chen, *Biomaterials.,* 2014, **35**, 5393.
37 H. Y. Nie, W. Guo, Y. Yuan, Z. P. Dou, Z. J. Shi, Z. Liu, H. F. Wang and Y. F. Liu, *Nano Res.,* 2010, **3**, 103.
38 D. W. Cao, S. Q. Tian, H. Huang, J. H. Chen and S. Pan, *Mol. Pharm.,* 2015, **12**, 240.
39 Z. Y. Xu, S. J. Zhu, M. W. Wang, Y. J. Li, P. Shi and X. Y. Huang, *ACS Appl. Mater. Interfaces.,* 2015, **7**, 1355.
40 X. Y. Zhang, C. K. Fu, L. Feng, Y. Ji, L.Tao, Q. Huang, S. X. Li and Y. Wei, *Polymer.,* 2012, **53**, 3178.

41 X. Y. Zhang, S. Q.Wang, C. K. Fu, L. Feng, Y. Ji, L. Tao, S. X. Li and Y. Wei, *Polym. Chem.,* 2012, **3**, 2716.
42 D. X. Wang, Y. L. Tong, Y. Q. Li, Z. M. Tian, R. X. Cao and B. S.Yang, *Diam. Relat. Mater.,* 2013, **36**, 26.
43 Y. Dong, R. X. Cao, Y. Q. Li, Z. Q. Wang, L. Li, and L. Tian, *RSC. Adv.,* 2015, **5**, 82711.
44 V. P. Podduturi, I. B. Magana, D. P. O'Neal and P. A. Derosa, *Comput. Meth. Prog. Bio.,* 2013, **112**, 58.
45 Y. Q. Li, Y. L. Tong, R. X. Cao, Z. M. Tian, B. S. Yang and, P. Yang, *Int. J. Nanomed.,* 2014, **9,** 1065.
46 S. Chae, H. Kim, M. S. Lee, Y. L. Jang, Y. Lee, S. H. Lee, K. Lee, S. H. Kim, H. T. Kim, S. C. Chi, T. G. Park and J. H. Jeong, *Macromol. Biosci.,* 2011, **11**, 1169.
47 T. Iversen, T. Skotland and K. Sandvig, *Nano Today.,* 2011, **6**, 176.
48 B. D.Chithrani and W. C. W. Chan, *Nano Lett.,* 2007, **7**, 1542.
49 H. C. Reinhardt, P. Hasskamp, I. Schmedding, S. Morandell, M. A. T. M. van Vugt, X. Z. Wang, R. Linding, S. E. Ong, D. Weaver, S. A. Carr and M. B. Yaffe, *Mol. Cell.,* 2010, **40**, 34.
50 F. Danhier, O. Feron and V. Preat, *J. Control. Release.,* 2010, **148**, 135.
51 A. S. Narang and S. Varia, *Adv. Drug Deliver. Rev.,* 2011, **63**, 640.